

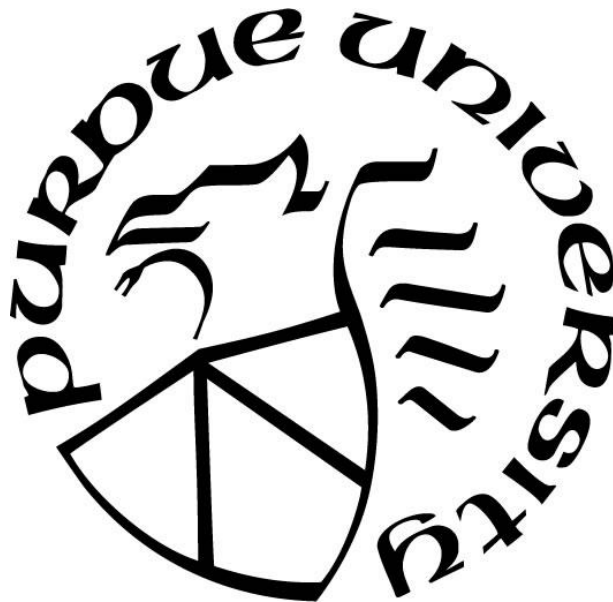
**DECOMPOSITION OF AMMONIUM PERCHLORATE ENCAPSULATED
NANOSCALE AND MICRON-SCALE CATALYST PARTICLES**

by
Spencer Fehlberg

A Thesis

*Submitted to the Faculty of Purdue University
In Partial Fulfillment of the Requirements for the degree of*

Master of Science in Mechanical Engineering



School of Mechanical Engineering

West Lafayette, Indiana

May 2020

**THE PURDUE UNIVERSITY GRADUATE SCHOOL
STATEMENT OF COMMITTEE APPROVAL**

Dr. Steven F. Son, Chair

School of Mechanical Engineering

Dr. Terrence R. Meyer

School of Aeronautics and Astronautics

Dr. Christopher S. Goldenstein

School of Aeronautics and Astronautics

Approved by:

Dr. Nicole Key

For my family, my friends, and especially my wife.

ACKNOWLEDGMENTS

I would like to thank my advisor, Professor Steven Son, for helping to make me a better student, researcher and hopefully a better future employee. I would also like to thank my committee members, Dr. Chris Goldenstein and Dr. Terry Meyer for their help and support. My fellow researchers at Maurice J. Zucrow Laboratories and the Purdue Energetics Research Center also deserve a special thanks for helping me more than I could have ever asked them to.

I also would like to thank the many friends and family members who encouraged me to keep going and helped me to stay optimistic even when disappointments came. I don't know if I could have done it without you all.

TABLE OF CONTENTS

LIST OF TABLES	6
LIST OF FIGURES	7
LIST OF ABBREVIATIONS.....	8
ABSTRACT.....	9
1. INTRODUCTION	10
1.1 Background.....	10
2. EXPERIMENTAL METHODS	12
2.1 Crystal Preparation Methods.....	12
2.2 Characterization Methods	13
3. RESULTS	15
3.1 Encapsulation Results	15
3.2 Thermal Decomposition Results.....	17
3.3 Hot-Stage and Micro-CT Analyses.....	20
4. CONCLUSIONS	26
REFERENCES	28
VITA.....	30

LIST OF TABLES

Table 1.1. DSC curve maxima for fine AP with iron oxide.	19
Table 1.2. DSC curve maxima for coarse AP with iron oxide	16

LIST OF FIGURES

Figure 1.1. Encapsulated particles, a) AP-encapsulated nanoscale particles, b) AP-encapsulated micron-scale particles, c) AP-encapsulated nanoscale catalyst particles that have been grown, d) and AP-encapsulated micron-scale catalyst particles that have been grown.	15
Figure 1.2. Examples of using the filtrate for verification methods: a) micron-scale catalyst encapsulation, b) successful micron-scale catalyst encapsulation.	16
Figure 1.3. Comparison of physical mixture with encapsulated particles in hexanes for a) nanoscale catalyst particles physically mixed with AP, b) AP-encapsulated nanoscale catalyst particles, c) micron-scale catalyst particles physically mixed with AP, and d) AP-encapsulated micron-scale catalyst particles.	16
Figure 1.4. Closed-pan DSC plots of fine particles: a) AP-encapsulated nanoscale catalyst particles, b) AP-encapsulated micron-scale catalyst particles.	18
Figure 1.5. Closed-pan DSC plots of coarse particles: a) grown AP-encapsulated nanoscale catalyst particles, b) grown AP-encapsulated micron-scale catalyst particles.	19
Figure 1.6. Microscope images of AP-encapsulated nanoparticles during heating.	21
Figure 1.7. Digital microscope images of coarse neat AP during heating from room temperature to 500 °C in the hot-stage.	22
Figure 1.8. Microscope images of grown AP-encapsulated micron-scale catalyst particles as the particles were heated from room temperature to 500 °C in the hot-stage.	22
Figure 1.9. Gray-scale reconstructed scans of grown AP-encapsulated micron-scale catalyst particles.	23
Figure 1.10. Sectioned views of the AP crystal from Figure 9 after heating to various temperatures. Note that the faintness of iron concentrations at room temperature is due to post-processing to reduce ring artifacts in that individual scan.	24
Figure 1.11. 3D models of the crystal in Figs. 9-10 using Avizo® software. The top row shows the features visible on the surface of the particle. The bottom row shows the same particle with the AP set to semi-transparent.	25

LIST OF ABBREVIATIONS

AP	Ammonium perchlorate
DSC	Digital Scanning Calorimetry
CT	Computed tomography

ABSTRACT

Iron oxide is the most common catalyst in solid rocket propellant. We have previously demonstrated increased performance of propellant by encapsulating iron oxide particles within ammonium perchlorate (AP), but only nanoscale particles were used, and encapsulation was only accomplished in fine AP (~20 microns in diameter). In this study, we extended the size of particle inclusions to micron-scale within the AP particles as well the particle sizes of the AP-encapsulated catalyst particles (100s of microns) using fractional crystallization techniques with the AP-encapsulated particles as nucleation sites for precipitation. Here we report catalyst particle inclusions of micron-scale, as well as nanoscale, within AP and present characterization of this encapsulation. Encapsulating micron-sized particles and growing these composite particles could pave the way for numerous possible applications. A study of the thermal degradation of these AP-encapsulated particles compared against a standard mixture of iron oxide and AP showed that AP-encapsulated micron-scale catalyst particles exhibited similar behavior to AP-encapsulated nanoscale particles. Using computed tomography, we found that catalyst particles were dispersed throughout the interior of coarse AP-encapsulated micron-scale catalyst particles and decomposition was induced within these particles around catalyst-rich regions.

1. INTRODUCTION

1.1 Background

The most common oxidizer used in solid rocket propellants is ammonium perchlorate. Often, a bimodal distribution of AP particle sizes is used for these composite propellants [1]. The bimodal distribution typically contains a mixture of coarse ($>100\ \mu\text{m}$ diameter) and fine ($<20\ \mu\text{m}$ diameter) particles [2-4]. As the coarse to fine ratio is changed, the flame structure changes, which results in different burning rates [5]. Further, adding a catalyst, such as iron (III) oxide (Fe_2O_3), reduces the surface activation energy for the decomposition reaction of AP and can also be used to tailor burning rates [6]. The highest propellant burning rate is seen when using nanoscale catalyst particles due to increased surface contact by the smaller particles [7-11]. However, increasing the catalyst amount beyond a certain point negatively impacts the propellant performance because it is an inert material in typical propellant reactions. Additionally, large amounts of fine particles increase the viscosity of the propellant to a point that makes it difficult to mix [12-13]. Encapsulating the catalyst particles averts this problem, and the ability to encapsulate nanoscale particles with AP has been demonstrated by multiple groups [14-15]. Additionally, the ability to encapsulate micron-sized particles, and to also grow those particles, may allow several other applications to be considered in future work with other materials as particle inclusions within the AP.

The encapsulation of micron-scale catalyst particles or the production of coarse AP particles with catalyst inclusions, to our knowledge, has not been performed prior to this study. In this study, we have encapsulated the nanoscale and micron-scale iron oxide particles within AP of varying particle sizes while averting the difficulty in propellant mixing that these catalyst particles create [5]. Moreover, the thermal decomposition of all encapsulated particles was also studied.

Characterization of these particles was focused on the decomposition of these particles under elevated temperatures from ambient to full decomposition temperatures. Digital microscopy, X-ray micro computed tomography (micro-CT), and differential scanning calorimetry (DSC) analyses were performed to fully characterize the encapsulated particles and were compared against neat AP and a physical mixture of AP and iron oxide exposed to the same experimental conditions. This work identifies what impact the encapsulation procedure has on the

decomposition of AP, observes the locations of the iron oxide within or around the AP, and observes the impact of catalyst position on the decomposition of the AP.

2. EXPERIMENTAL METHODS

2.1 Crystal Preparation Methods

Encapsulation of nanoscale particles was accomplished with a fast-crash solvent-antisolvent method, which is described in greater detail elsewhere [14]. In short, it can be summarized as follows: AP (1.5 g, RCS Rocket Motor Components, Cedar City, UT) was dissolved in acetone (100 mL, Fisher Scientific, Pittsburg, PA) chilled in an ice bath. Iron oxide particles (15 mg of 3 nm Fe₂O₃, Mach I Chemicals, King of Prussia, PA) were dispersed in the solution by immersing the container in a Marshall Scientific (Hampton, NH) Branson 2510 ultrasonic cleaner for five minutes. Ethyl acetate (300 mL, Fisher Scientific, Pittsburg, PA) antisolvent was added to this solution, causing the AP crystals to form nucleation sites around the iron oxide particles. The particles were then filtered from the solvent/antisolvent mixture, air dried, and placed in a container. The particles were then rinsed with hexanes (Alliance Chemical, Austin, TX), in a sonic bath and excess hexanes were pipetted away from the container. Rinsing with hexanes was performed three times before particles were dried in a vacuum.

These particles are grown to form coarse particles in a manner standard to the industry [15], which involves creating a saturated AP solution of AP (3.34 g, RCS Rocket Motor Components, Cedar City, UT) and distilled water (10.0 mL) at 60 °C, adding seed particles (1.00 g of AP-encapsulated nanoscale or micron-scale particles in our case), sonicating for 30 seconds with an ultrasonic cleaner and then reducing the temperature of the solution by 10 degrees to promote AP precipitation on the fine AP-encapsulated catalyst particles. The solution was maintained at this reduced temperature for at least four hours and stirred with a Happybuy (Beijing, China) 100W overhead stirrer mixer to allow for complete equilibration before the particles were separated from the mother liquor. A No. 140 (106 μm) stainless steel sieve (Cole-Parmer, Vernon Hills, IL) was used to separate the coarse particles from fine particles as well as to prevent agglomeration, and the sieved particles were rinsed with hexanes three times and dried in a vacuum. We modified the procedures described in the literature from industrial scale to 1-gram batches. For these reasons, the process was carried out over a shorter time period than in these systems with a smaller proportional yield of coarse AP. A size distribution analysis of micron-scale iron oxide (1-5 μm, Sigma Aldrich, St. Louis, MO) is given elsewhere [16].

All tests were performed with neat and physically mixed samples with identical AP and iron oxide particle sizes. Fine AP was produced by performing the encapsulation procedure without adding catalyst. Coarse AP (RCS Rocket Motor Components, Cedar City, UT) used was 106 μm in diameter and larger. Physical mixing was carried out by mixing the AP with 1% by weight catalyst in hexane with an ultrasonic bath for five minutes followed by evaporation of the hexanes.

2.2 Characterization Methods

In other works utilizing the encapsulation procedure [5,14], encapsulation was quantitatively validated of materials fabricated using similar methods. Here, encapsulation was verified on a qualitative basis. First, the color of the filtrate is used as a strong indicator of encapsulation success or failure. A high degree of encapsulation is indicated by a very clear filtrate. Filter paper was used to separate AP-encapsulated nanoscale and micron-scale particles from the solvent-antisolvent mixture respective mean pore sizes of 2.5 μm (Whatman 1442, GE Healthcare Bio-Sciences, Pittsburgh, PA) and 8.0 μm (Lab Nerd 6202, Avagadro's Lab Supply, Shamong, NJ), both of which are much larger than particles being encapsulated with AP. A clear filtrate indicates catalysts have been encapsulated and therefore do not pass through the filter. Examples of this verification method are shown in Figure 1.1. Another verification method involves the examination of the solution when the particles are mixed in a hexane solution. For each sample, 15.0 mg of particles were dispensed sonically in 2.0 mL of hexane and allowed to rest for five minutes. A cloudy solution indicates poor encapsulation. Physical mixtures are used as references.

DSC analyses were performed with heating from room temperature to 475 $^{\circ}\text{C}$ using a TA Instruments (New Castle, DE) Q600 with a heating rate of 10 $^{\circ}\text{C}/\text{min}$ under ultra-high purity argon (99.999%) at 100 mL/min with closed aluminum pans. A typical DSC profile of AP has three major events as associated with decomposition, in order of increasing temperature: first, an endothermic region associated with transition from orthorhombic to cubic phase [17] second, an exothermic energy release associated with low-temperature decomposition; and third, an endothermic or exothermic energy release associated with high-temperature decomposition. Cubic AP exhibits purely exothermic behavior in a closed pan, whereas endothermic behavior is observed in open pans [18]. While our previous work utilized open pan analysis [14], we have used closed pan analysis in this study to characterize the impact of encapsulation on all decomposition events.

Hot stage microscopy was performed using a Hirox (Hackensack, NJ) KH-8700 digital microscope coupled with a Linkam (Surrey, UK) TS1000 hot stage. Samples were heated from room temperature to 475 °C to replicate the heating rate used in the DSC analyses. A quartz pan was placed on top of a sapphire window to allow for closed pan testing in the hot stage.

Micro-CT scans were performed to identify the distribution and concentration of iron oxide particles inside the AP crystals. A Bruker (Kontich, Belgium) SkyScan 1272 with an operating voltage of 50 kV was employed with an aluminum 0.25 mm filter at a rotation step of 0.3°. The scanned images were reconstructed using NRecon software (Bruker, Kontich, Belgium) and analyzed using Avizo software (Thermo Fisher Scientific, Hillsboro, OR). The steps for analyzing each image in Avizo were the same, though settings were adjusted slightly to accommodate small variations in the images due to anomalies in scans, variations in scanner settings, and different reconstruction settings. A median filter was followed by interactive thresholding to distinguish AP and iron oxide particles from the surrounding free space and materials used to hold the sample in place during scanning. The crystal was then separated using the separate objects function. Segmentation was used to identify free space (pores) within the particles.

3. RESULTS

3.1 Encapsulation Results

Figure 1.1 shows the successfully encapsulated nanoscale and micron-scale catalyst particles. Catalyst-rich regions can be observed as dark specks or colored regions scattered throughout the crystals, showing that encapsulation of nanoscale and micron-scale catalysts was achieved. A small, but visible amount of catalyst loss occurred during the growing procedure of the fine AP-encapsulated catalyst particles, although the amount lost was not measured directly due to difficulty presented by working with a high-temperature aqueous solution of AP. Visual inspection suggested that the amount lost was much less than the amount retained, as was verified later using micro-CT techniques. Despite this apparent loss of catalyst particles, the remaining particles are clearly dispersed throughout the AP particles.

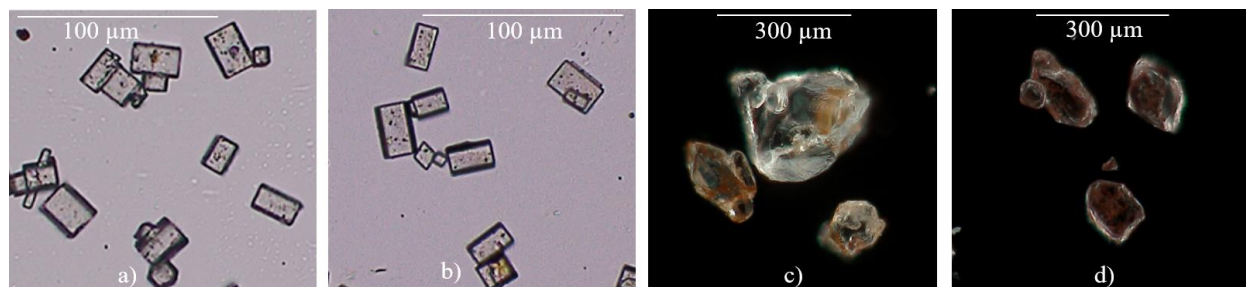


Figure 3.1. Encapsulated particles, a) AP-encapsulated nanoscale particles, b) AP-encapsulated micron-scale particles, c) AP-encapsulated nanoscale catalyst particles that have been grown, d) and AP-encapsulated micron-scale catalyst particles that have been grown.

Verification methods of the fine AP-encapsulated catalyst particles showed that AP-encapsulated micron-scale catalyst particles retained a similar amount of iron oxide particles as AP-encapsulated nanoparticles (Figures 1.2-1.3).

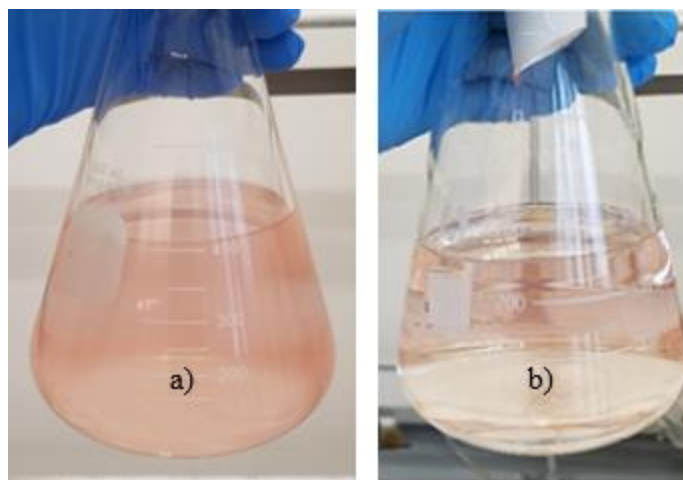


Figure 3.2. Examples of using the filtrate for verification methods: a) micron-scale catalyst encapsulation, b) successful micron-scale catalyst encapsulation.

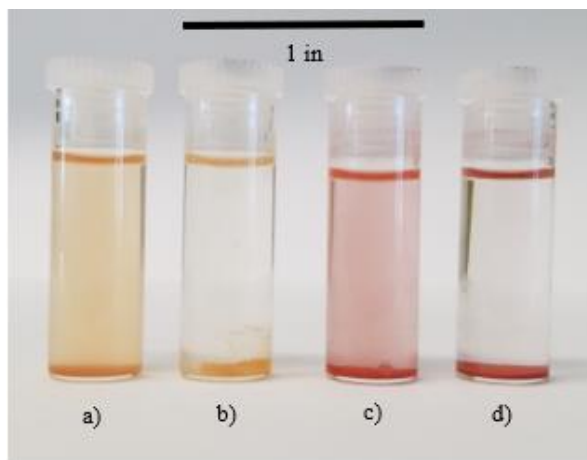


Figure 3.3. Comparison of physical mixture with encapsulated particles in hexanes for a) nanoscale catalyst particles physically mixed with AP, b) AP-encapsulated nanoscale catalyst particles, c) micron-scale catalyst particles physically mixed with AP, and d) AP-encapsulated micron-scale catalyst particles.

Although these are qualitative measurements, they clearly show that encapsulation has occurred. Figure 1.2 shows that when encapsulated in AP, very few iron oxide particles pass through the filter paper. The AP particles are much larger than the iron oxide particles, and therefore settle in solution much more rapidly than the iron oxide particles as shown in Figure 1.3. By inspecting the bottom of the vials, one can observe that a similar amount of material has

accumulated, but the overall transparency is vastly different between the physical mixtures and the encapsulated particles.

3.2 Thermal Decomposition Results

DSC curves of fine and coarse particles in Figures 1.4-1.5 with a) neat, b) physically mixed with iron oxide (1% by weight), and c) AP-encapsulated iron oxide. Analysis of local maxima are summarized in Tables 1 and 2 for these samples. These tests were performed multiple times, and percent variations in local maxima for each sample are also shown in the tables.

Previous work was performed with open pans and exhibited mass depletion (corresponding to the second exothermic peak) occurring nearly 55°C below the neat or physically mixed samples at a temperature of ca. 360 °C [14]. The results shown here indicate that in a closed-pan test, the DSC curves of AP-encapsulated nanoscale catalysts and physical mixture of AP with nanoscale catalyst have maxima occurring at roughly the same temperatures (Figure 1.4a) and the decomposition of encapsulated particles ends 16 °C higher than our previous open-pan analysis [14]. However, the first exotherm of the AP-encapsulated micron-scale catalyst particles (Figure 1.4b) is 9°C lower than the physical mixture. This corresponds to a difference of 3.0% of the physical mixture value, well outside the highest observed variation of the first exotherm of 0.7%. The second exotherm has a similar effect, though its reduction is 1.9% of the physical mixture temperature and the largest variance of the second exotherm is 1.4%. These results show that confinement has a clear impact on the decomposition of these particles, though this impact seems to be dependent on the size of catalyst inclusions in the AP. Thermogravimetric analysis was used to determine average final mass content (as a percent of initial). When comparing encapsulated catalyst particles and grown AP-encapsulated catalyst particles with their corresponding physical mixtures, we found a difference of less than 1.0% which was determined to be insignificant.

Coarse AP-encapsulated catalyst particles did not exhibit consistent decomposition behavior in the exothermic region, but this may be due to multiple effects. Catalyst particles were visibly lost from the crystals during the growth procedure, and variations in the catalyst retention amounts likely has a strong impact on decomposition. Because crystallization is a purification process, and the encapsulated particles are essentially contaminants in the AP crystalline structure, it is expected that some iron oxide will not be maintained in the crystalline structure. A characterization of how much iron oxide is lost during this process was not performed because the purpose of this work

was to establish the capability to create coarse AP particles with catalyst inclusions but may be of value in future work. Physical mixtures of these particles contained the same 1% weight as the fine particles. Further, as the particles grow, AP is deposited on the outside of the AP-encapsulated catalyst particles. This may create a “core-shell” effect and separates the catalyst particles from increased amounts of AP. We intentionally selected single particles for this analysis, but we did not resolve their structure to ensure that they were not polycrystalline. A more complex structure created by polycrystallinity may result in different decomposition behavior and could also contribute to the decomposition behavior observed in Fig. 5 and may be a valuable study for future work.

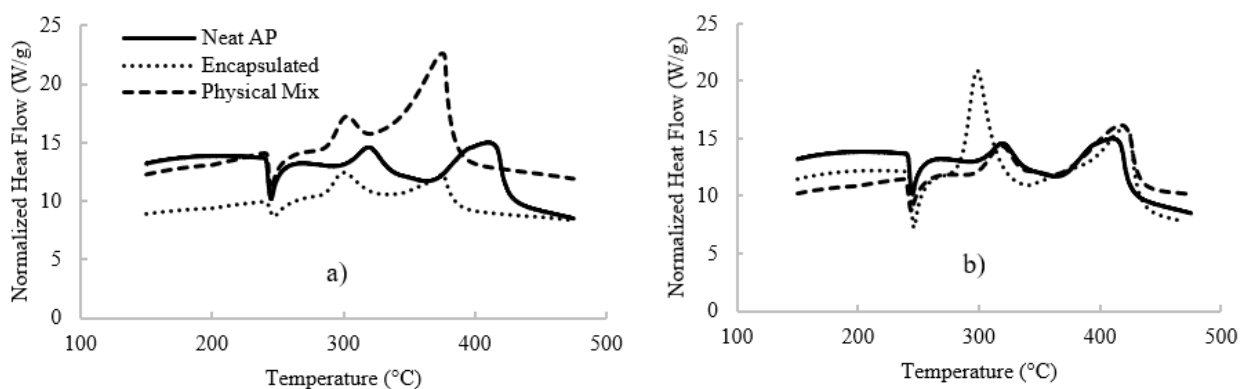


Figure 3.4. Closed-pan DSC plots of fine particles: a) AP-encapsulated nanoscale catalyst particles, b) AP-encapsulated micron-scale catalyst particles. The same data is used for neat AP in both plots and can be used as a reference point for comparison.

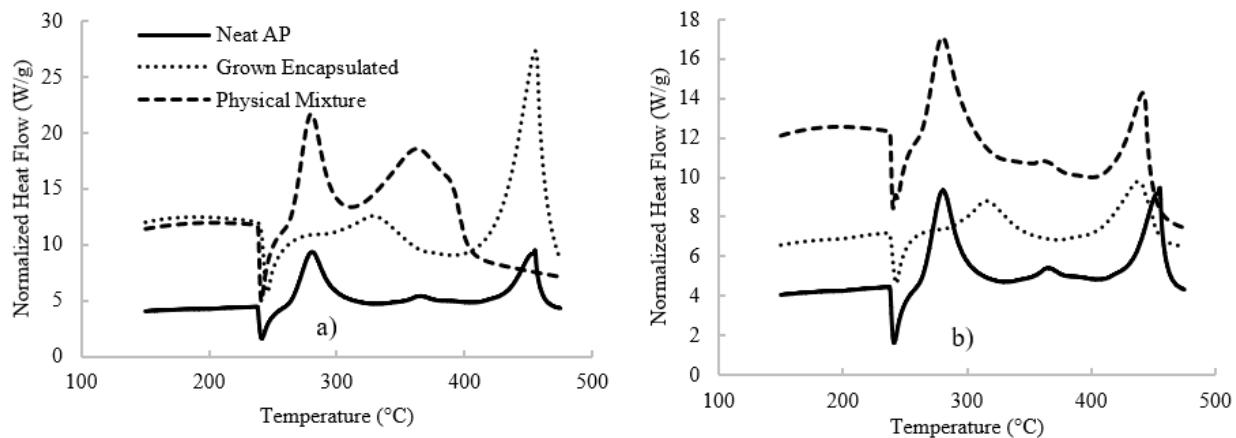


Figure 1.5. Closed-pan DSC plots of coarse particles: a) grown AP-encapsulated nanoscale catalyst particles, b) grown AP-encapsulated micron-scale catalyst particles. The same data is used for neat AP in both plots and can be used as a reference point for comparison.

Table 3.1. DSC curve maxima for fine AP with iron oxide. Percent variances are shown in parentheses.

Local Maximum	Neat AP	Nanoscale Encapsulated	Nanoscale Physical Mixture	Micron-scale Encapsulated	Micron-scale Physical Mixture
Endothermic Peak (°C)	245 (0.1%)	247 (0.8%)	245 (0.4%)	246 (0.4%)	244 (0.0%)
First Exothermic Peak (°C)	320 (0.6%)	301 (0.3%)	311 (0.3%)	299 (0.7%)	319 (0.3%)
Second Exothermic Peak (°C)	413 (1.1%)	376 (1.3%)	375 (0.2%)	420 (0.2%)	419 (1.4%)

Table 3.2. DSC curve maxima for coarse AP with iron oxide. Percent variances are shown in parentheses.

Local Maximum	106 μm Neat AP	106 μm Grown AP-Encapsulated Nanoscale Catalyst	106 μm AP and Nanoscale Catalyst Physical Mixture	106 μm Grown AP-Encapsulated Micron-Scale Catalyst	106 μm AP, and Micron-scale Catalyst Physical Mixture
Endothermic Peak ($^{\circ}\text{C}$)	241 (0.4%)	243 (0.4%)	241 (0.4%)	243 (0.4%)	240 (0.8%)
First Exothermic Peak ($^{\circ}\text{C}$)	281 (0.0%)	315 (0.3%)	280 (0.1%)	315 (0.6%)	280 (0.3%)
Second Exothermic Peak ($^{\circ}\text{C}$)	455 (1.3%)	430 (1.6%)	363 (1.1%)	439 (0.1%)	441 (0.4%)

3.3 Hot-Stage and Micro-CT Analyses

A hot stage is essentially a small oven with viewports. In this study, this device was used with digital backlit microscopy to generate images of the decomposition as it occurred. In order to simulate a closed pan, a quartz pan was placed on top of a sapphire window. The thermal degradation of these samples is shown in Figs. 6-8. Figure 1.6 shows AP-encapsulated nanoparticles while heating. In the case of the encapsulated particles, no changes in the particles were seen from room temperature until about 245 $^{\circ}\text{C}$. At this point, warping and movement of the crystals associated with a volume expansion indicated transition from orthorhombic to cubic crystalline structure occurred [17]. Opaque regions were seen propagating from iron oxide rich regions concentration near 270 $^{\circ}\text{C}$, indicative of the onset of low-temperature decomposition. Following this, the crystal structures begin to rapidly deteriorate as the particles transition into high-temperature decomposition, and the crystals eventually disintegrate and leave only catalyst remnants around 400 $^{\circ}\text{C}$ as previously reported [18]. A neat AP decomposition follows a similar process but transition from clear to opaque appears to spread throughout the crystals in a fairly even manner. Eventually the particles begin to decompose at the edges and begins to gradually retreat.

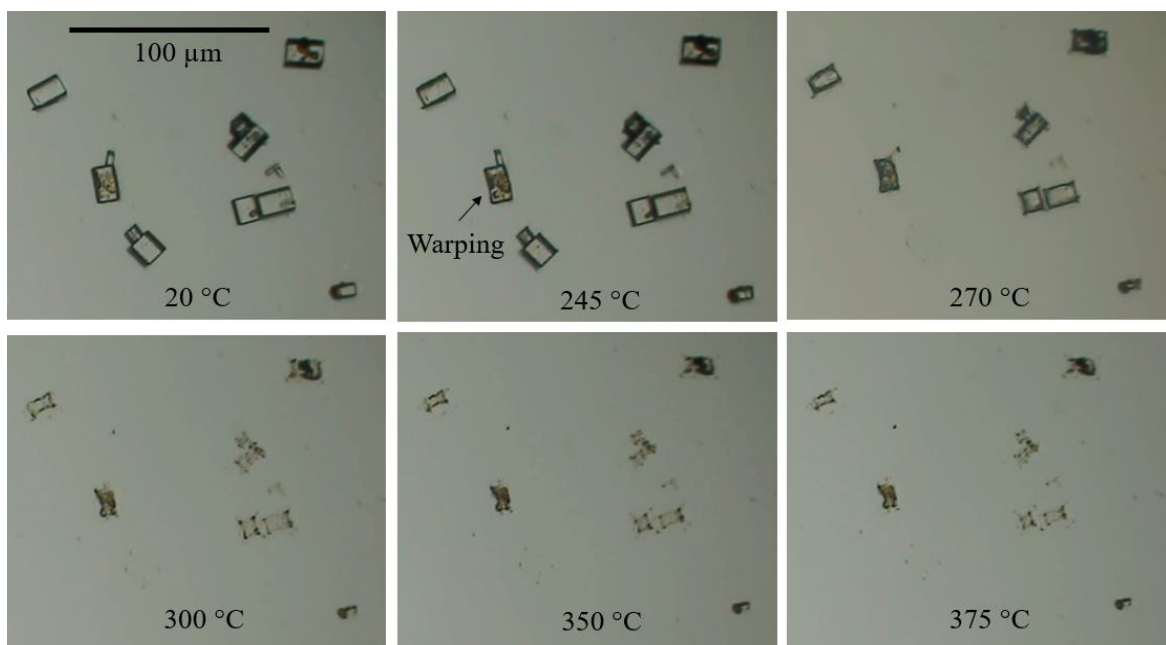


Figure 1.6. Microscope images of AP-encapsulated nanoparticles during heating.

Analysis of the coarse particles provides greater perspective into the decomposition process. Images of neat AP are shown in Figure 1.7 and grown encapsulated micron-scale particles are shown in Figure 1.8. Phase transition begins at nearly the same temperature as fine particles, but it takes longer to spread throughout each particle. Neat AP gradually begins to darken (indicative of degradation) but does not appear to have a specific location where this process is concentrated. In the grown encapsulated particles, however, dark spots are concentrated in specific locations. In the Figure 1.8, this process begins in a region where no surface defects are seen indicating that the decomposition process begins inside the particle. This dark spot spreads while other such regions begin forming and continues to grow until rapid decomposition begins occurring around 330 °C. Large amounts of gas generated around 340 °C prevented further observations from being made, but it was apparent at this point that the particle was collapsing on itself and complete disintegration of the particle was underway.

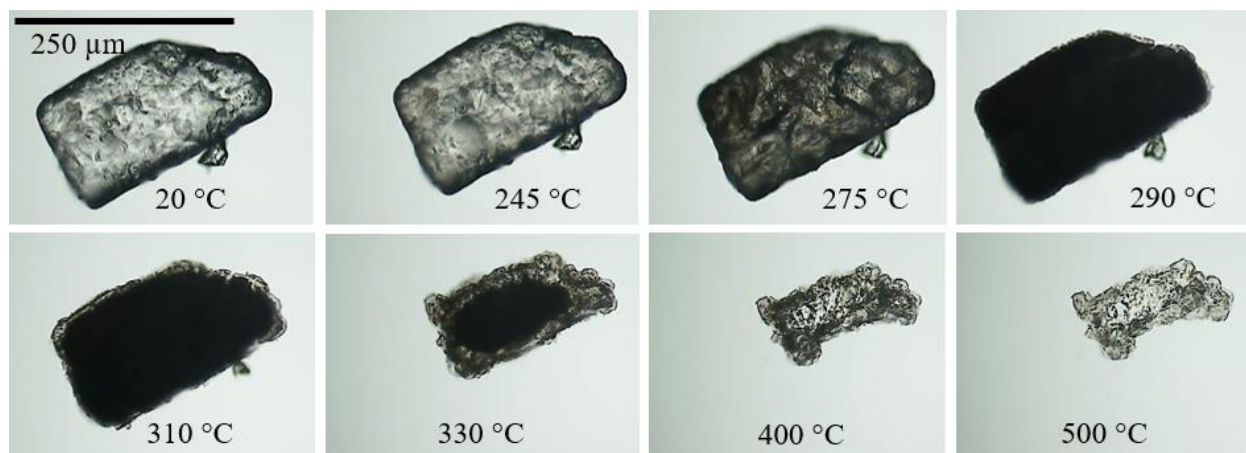


Figure 1.7. Digital microscope images of coarse neat AP during heating from room temperature to 500 °C in the hot-stage.

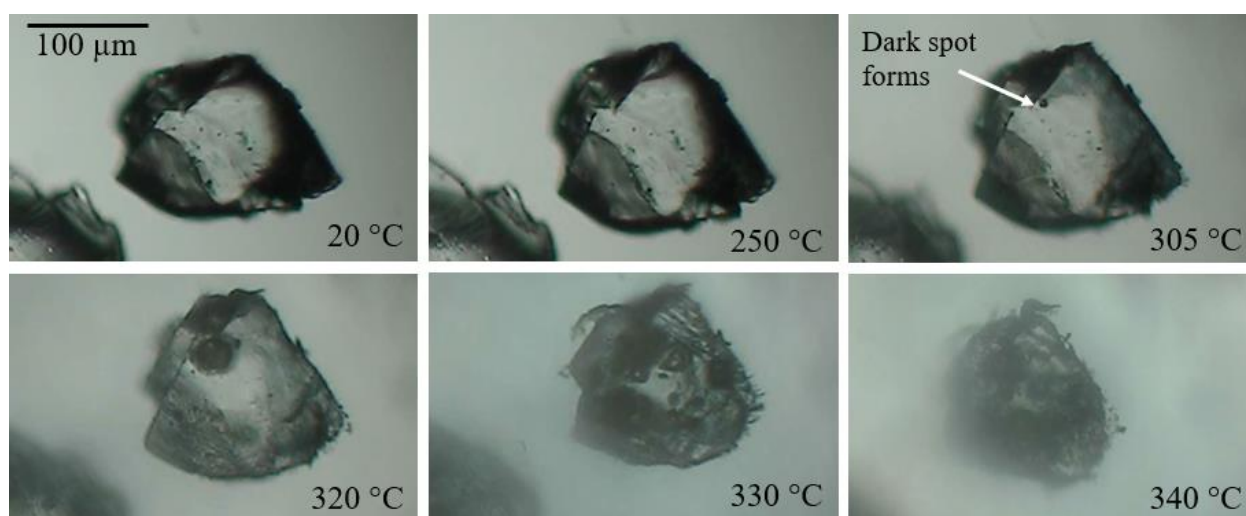


Figure 1.8. Microscope images of grown AP-encapsulated micron-scale catalyst particles as the particles were heated from room temperature to 500 °C in the hot-stage.

Micro-CT analysis was attempted on coarse and fine AP-encapsulated particles, but only coarse particles were able to be satisfactorily processed. As the size of object being scanned decreases, the sensitivity to various scanning parameters become more significant, making scans of fine particles much more difficult. Future work will be devoted to exploring these parameters in order to analyze fine particles. For the purposes of this work, we focused on the analysis of coarse AP particles. Figs. 9-10 show reconstructed micro-CT images of grown AP-encapsulated micron-scale catalyst particles. An initial scan at room temperature was followed by heating the particles to multiple temperatures, with a CT scan after each heating event. Particles were heated

with the hot stage with a 10 °C/min and held at each temperature for 5 minutes before cooling to room temperature without forced cooling. The areas of highest density are brightest color – these indicate catalyst-rich regions. Figure 1.9 shows how the AP warps during heating above 245 °C due to phase transformation. Cracks form in the AP as a result of this process and are visible on the surface of the crystal.

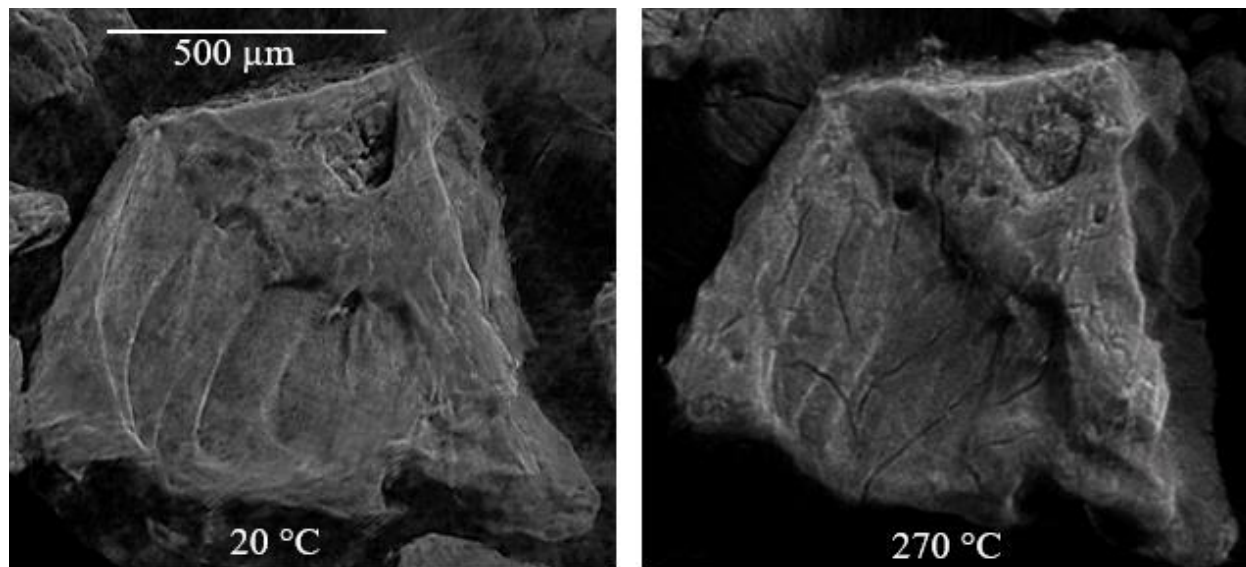


Figure 1.9. Gray-scale reconstructed scans of grown AP-encapsulated micron-scale catalyst particles.

Sections, shown in Figure 1.10, reveal iron concentrations within the crystal and show decomposition. Note that the scale bars represent a length of 500 μm , which is far larger than the mean iron oxide particle size of 1.0 μm . The most visible concentrations of iron oxide particles, therefore, are agglomerates of these particles. Though there are apparent voids in the particle prior to heating, the number of voids increases steadily with temperature. At 305 °C, after low-temperature decomposition has begun, voids begin to appear around the iron oxide concentrations. This continues at higher temperatures, and porosity increase throughout the particle is observed visually. Smaller iron oxide concentrations are suspected to be present at these locations. Further, the relative size of the particle has not changed significantly. These results agree closely with those observed in the hot stage analysis performed. Note that the catalyst particles appear to change slightly in size – this is an image artifact resulting from the decomposition of AP near these particles.

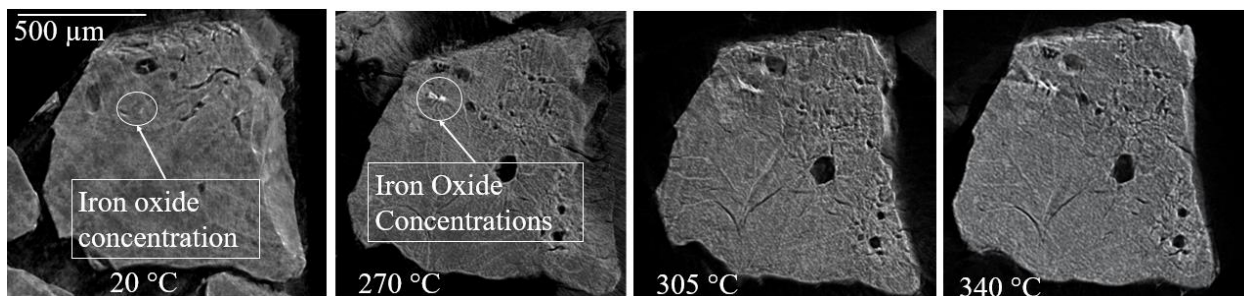


Figure 1.10. Sectioned views of the AP crystal from Figure 1.9 after heating to various temperatures. Note that the faintness of iron concentrations at room temperature is due to post-processing to reduce ring artifacts in that individual scan.

Additional 3D processing with Avizo software yields further insights and is shown in Figs. 10-11. Setting the AP to semi-transparent (second row of Figure 1.11) reveals pores and iron oxide within the AP. The brightest red and darkest black represent iron oxide and pores closest to the surface, respectively.

Figure 1.11 shows that there are voids in the particle prior to heating, though most of them are near the surface. It also shows that there is iron oxide dispersed throughout the particle. After heating to 270 °C, iron oxide concentrations are less apparent (though still present) due to a large increase in surface porosity. Cracks are visible on the surface due to heating and cooling past the region of phase transformation. After heating to 305 °C, the particle has passed through the first exothermic region of decomposition. This is evidenced by the surface of the crystal becomes slightly more porous, and the inside becomes significantly more porous. Iron oxide particles are also closer to the surface. The particle decreased slightly in size. After heating to 340 °C, the surface and the inner sections of the particle have become significantly more porous and more of the iron oxide is near the surface as the particle has decreased further in size. Of greatest significance is the observation that porosity is increasing in areas of iron oxide concentration which are located within the AP.

Closed porosity calculations are also included in Figure 1.11. Though the initial calculated porosity appears to be quite high, this is mostly a product of the irregular size and surface of the particle which make closed porosity calculations difficult. These results are best interpreted by observing the large increase in porosity as the particle begins to experience thermal decomposition that clearly favors concentrations of iron oxide. Avizo was also used to estimate the iron oxide concentration by volume, which was then used to calculate a mass concentration of 0.82%.

Because the iron oxide particles have a mean diameter on the order of the resolution of the scanner, the overall concentration may be higher.

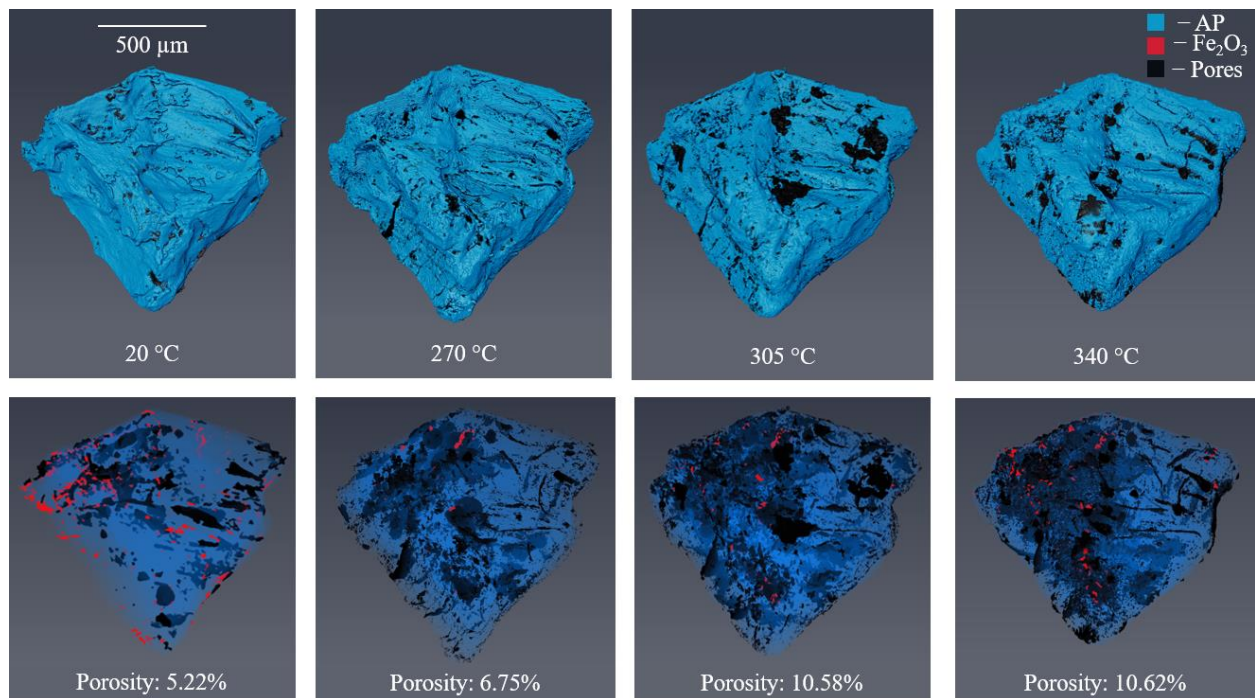


Figure 1.11. 3D models of the crystal in Figs. 9-10 using Avizo software. The top row shows the features visible on the surface of the particle. The bottom row shows the same particle with the AP set to semi-transparent.

4. CONCLUSIONS

Micron-scale catalyst particles were encapsulated within AP crystals with a fast-crash solvent/antisolvent method. These particles, along with AP-encapsulated nanoscale iron oxide, were subjected to multiple studies to characterize their thermal degradation and were compared against neat AP and physical mixtures of AP with the two different sizes of iron oxide.

DSC analysis of fine particles showed that the impact of encapsulated catalyst is diminished when closed pan samples are used as compared to open pan testing used in previous work. When an open pan is used rather than a closed pan, gaseous products are more readily removed from the reaction area following the first exothermic reaction. Condensed phase reactions dominate, and an endothermic region is observed. Conversely, gas phase reactions dominate during a closed pan test, resulting in a second exothermic region, and iron oxide is less able to catalyze these reactions [18]. In the first exothermic region, which has the same reaction behavior in both open and closed pan experiments, the encapsulated micron-scale particles were observed to have a significant impact on the reaction when compared to the physically mixed samples. The reason that a similar effect was not observed with AP-encapsulated nanoscale catalyst particles may be due to the relative size of the catalyst particles. Their proximity to the surface of the particles may be greater, inhibiting their ability to contribute to the gas-phase reaction. The crystal structure of the catalyst particles may also have an impact on these results. The manufacturer states that the nanoscale catalyst particles used have an amorphous crystal structure. This crystal structure has only been observed in particles less than 5 nm in diameter, whereas the micron-scale particles have a rhombohedral centered hexagonal structure [19].

The nature of the condensed-phase reaction, combined with significant losses of iron oxide during the growing procedure of coarse AP crystals, may be the reason similar trends were not observed in the DSC curves of coarse particles. Improvements in the procedure may result in higher retention of iron oxide, which is expected to result in greater catalyzation. Additionally, polycrystalline effects resulting from the synthesis of coarse AP-encapsulated catalyst particles may be another contributing reason that these trends were not observed in the DSC curves of coarse particles.

Digital microscope images of particles while being heated in a hot-stage offered additional insights. Visible transition from orthorhombic to cubic phase was observed between 245 °C and

250 °C. The degradation process was observed to begin faster with samples containing encapsulated iron oxide. It appeared to begin around areas of high concentration in fine AP crystals and from within coarse AP crystals. Observations are limited after the particles transitioned from low-temperature decomposition to high temperature decomposition, but iron oxide remnants were still visible following the full decomposition process. Micro-CT analysis of coarse AP-encapsulated micron-scale catalyst particles confirmed that iron oxide was dispersed throughout the inside of the particles, not concentrated on the surface, and that decomposition occurs at these particles. This work not only gives insight to how decomposition proceeds with encapsulated catalysts. It also shows that micron catalyst particles can be encapsulated. This is significant because other applications for larger encapsulated particles, such as the inclusion of thermographic phosphors or microwave absorbing particles that will likely need to be micron-scale. In addition, we have demonstrated that larger AP particles with encapsulated catalysts can be produced.

REFERENCES

- [1] Stephens, M., Sammet, T., Petersen, E., “Performance of Ammonium-Perchlorate-Based Composite Propellant Containing Nanoscale Aluminum,” *Journal of Propulsion and Power*, Vol. 26, No. 3, May-June 2010, pp. 461-466. doi: 10.2514/1.45148
- [2] Chakravarthy, S. R., Seitzman, J. M., Lillard, R., Price, E. W., Sigman, R. K., “Intermittent Burning and Its Contribution to Plateau Burning of Composite Propellants,” 39th Aerospace Sciences Meeting and Exhibit, AIAA Paper 2001-0339, Reno, NV, Jan. 2001. doi: 10.2514/6.2001-339
- [3] Fitzgerald, R.P., Brewster, M. Q., “Flame and Surface Structure of Laminate Propellants with Coarse and Fine Ammonium Perchlorate,” *Combustion and Flame*, Vol. 136, No. 3, Feb 2004, pp. 313-326. doi: 10.1016/j.combustflame.2003.10.008
- [4] Ide, K. M., “Composite Propellants with Bi-Plateau Burning Behaviour,” Weapons Systems Div., Defence Science and Technology Organisation, Rept. DSTG-GD-0344, Edinburgh, Australia, 2002.
- [5] Isert, S., Groven, L. J., Lucht, R. P., Son, S. F., “The Effect of Encapsulated Nanosized Catalysts on the Combustion of Composite Solid Propellants,” *Combustion and Flame*, Vol. 162, No. 5, May 2015, pp. 1821-1828. doi: 10.1016/j.combustflame.2014.11.040
- [6] Chakravarthy, S. R., Price, E. W., Sigman, R. K., “Mechanism of Burning Rate Enhancement of Composite Solid Propellants by Ferric Oxide,” *Journal of Propulsion and Power*, Vol. 13, No. 4, 1997, pp. 471-480. doi: 10.2514/2.5208
- [7] Chaturvedi, S., Dave, P. N., “Nano-Metal Oxide: Potential Catalyst on Thermal Decomposition of Ammonium Perchlorate,” *Journal of Experimental Nanoscience*, Vol. 7, No, 2, 2012, pp. 205-231. doi: 10.1080/17458080.2010.517571
- [8] Hedman, T.D., Reese, D.A., Cho, K.Y., Groven, L.J., Lucht, R.P., Son, S.F., “An Experimental Study of the Effects of Catalysts on an Ammonium Perchlorate Based Composite Propellant Using 5 kHz PLIF,” *Combustion and Flame*, Vol. 159, No. 4, April 2012, pp. 1748–1758. doi: 10.1016/j.combustflame.2011.11.014
- [9] Ma., Z.Y., Li, F. S., Bai, H. P., “Preparation and Thermal Decomposition Behavior of Fe₂O₃/Ammonium Perchlorate Composite Nanoparticles,” *Acta Chimica Sinica*, Vol. 62, No. 13, Jul. 2004, pp. 1252-1255.

- [10] Joshi, S., Patil, P., Krishnamurthy, V., "Thermal Decomposition of Ammonium Perchlorate in the Presence of Nanosized Ferric Oxide," *Defence Science Journal*, Vol. 58, No. 6, 2008, pp. 721-727. doi: 10.14429/dsj.58.1699
- [11] Jain, S., Mehilal, M., Nandagopal, S., Singh, P., Radhakrishnan, K., Bhattacharya, B., "Size and Shape of Ammonium Perchlorate and their Influence on Properties of Composite Propellant," *Defence Science Journal*, Vol. 59, No. 3, 2009, pp. 294-299. doi: 10.14429/dsj.59.1523
- [12] Dokhan, A., Price, E. W., Seitzman, J. M., Sigman, R. K., "The effects of bimodal aluminum with ultrafine aluminum on the burning rates of solid propellants," *Proceedings of the Combustion Institute*, Vol. 29, No. 2, 2002, pp. 2939-2946. 30th International Symposium on Combustion, Chicago, IL, 25-30 Jul 2004. doi: 10.1016/S1540-7489(02)80359-5
- [13] Ciepluch, C. C., "Status of the 260-inch Diameter Solid Rocket Motor Program," *Second Solid Propulsion Conference, Interagency Chemical Rocket Propulsion Group and AIAA*, Anaheim, CA, June 6-8, 1967.
- [14] Reese, D. A., Son, S. F., Groven, L. J., "Preparation and Characterization of Energetic Crystals with Nanoparticle Inclusions," *Propellants, Explosives, Pyrotechnics*, Vol. 37, No. 6, Nov 2012, pp. 635-638. doi: 10.1002/prop.201200142
- [15] Kralik, R. J. et al, "Crystallization of Large Particle Sized Ammonium Perchlorate," US Patent 3,383,180, 1968.
- [16] Karlsson, H. L. et al, "Size-Dependent Toxicity of Metal Oxide Particles—A Comparison Between Nano- and Micrometer Size," *Toxicology Letters*, Vol. 188, 2009, pp. 112-118. doi: 10.1016/j.toxlet.2009.03.014
- [17] Shen, S. Chen, S., Wu, B., "The Thermal Decomposition of Ammonium Perchlorate (AP) Containing a Burning-Rate Modifier," *Thermochimica Acta*, Vol 223, 1993, pp. 135-143.
- [18] Vyazovkin, S., and Wight, C. A., "Kinetics of Thermal Decomposition of Cubic Ammonium Perchlorate," *Chemistry of Materials*, Vol 11, 1999, pp. 3386-3393.
- [19] Aboril, R., Mashlan, M., Petridis, D., "Iron (III) Oxides from Thermal Processes: Synthesis, Structural and Magnetic Properties, Mössbauer Spectroscopy Characterization, and Applications," *Chemistry of Materials*, Vol 14, 2002, pp. 969-982. doi: 10.1021/cm0111074

VITA

Spencer Allen Fehlberg

spencer.fehlberg@gmail.com

(801)888-3722

EDUCATION

MS Mechanical Engineering Student, *Purdue University*, West Lafayette, IN

May 2020

- 3.53 Cumulative GPA

BS Mechanical and Aerospace Engineering Student, *Utah State University*, Logan, UT

May 2018

- 3.88 Cumulative GPA
- *Magna Cum Laude*

RESEARCH AND INTERNSHIP EXPERIENCE

Graduate Research Assistant, *Maurice J. Zucrow Labs*, West Lafayette, IN

Jul 2018

– Current

- Developed fine and coarse energetic-encapsulated materials for multifunctional capabilities
- Characterized the thermal decomposition of coarse and fine AP-encapsulated iron oxide with nanoscale and micron-scale catalyst inclusions
- Research advisor: Prof. Steven F. Son

Design Engineering Intern, Aerojet Rocketdyne, Huntsville, AL May –

Aug 2019

- Modeled systems and created drawing packages
- Created finite element models of test articles for material characterization and performance prediction

Undergraduate Research Assistant, Utah State University Propulsion Lab, Logan, UT Jan

2017 – Jun 2018

- Discovered novel technique for electroplating nickel onto ABS plastic for use as hybrid rocket propulsion systems
- Developed aerospike nozzle thrust vectoring system
- Assisted in the testing of hybrid rocket motors

Research Associate, NASA Marshall Space Flight Center, Huntsville, AL May –

Aug 2017

- Designed the spin-up system of the final stage of a small launch vehicle
- Designed nozzle and analytically estimated performance in near-vacuum conditions, designed and tested ignition circuit, wrote LabVIEW code for testing spin-up system

Engineering Intern, Orbital ATK, Clearfield, UT May –

Aug 2016

- Involved in the process of manufacturing composite rocket motor casings
- Accomplished database clean-up, process improvement (tooling research and procurement), 5S of production area, procedure revision

Engineering Intern, HyperComp Engineering, Brigham City, UT May
2015 – Jan 2016

- Tested and constructed high-pressure COPVs

LEADERSHIP EXPERIENCE

Volunteer Coach, Purdue Cross Country Team, West Lafayette Indiana Sep
2018 – Current

- Coach both men's and women's cross country teams

Vice President, Tau Beta Pi, National Engineering Honor Society, Utah Gamma Chapter May
2017 – May 2018

- Planned and executed events to benefit the honor society and College of Engineering

Treasurer, Tau Beta Pi, National Engineering Honor Society, Utah Gamma Chapter May
2016–May 2017

- Coordinated with students and the Dean's Office to ensure involvement and funding

Volunteer Representative, The Church of Jesus Christ of Latter-Day Saints, West Virginia June 2012
– 2014

- Supervised 40 co-volunteers across three states to reach organizational goals

Senior Design Team Lead Engineer, Utah State University, Logan Utah Jan –
Dec 2017

- Designed a device for the recycling of lawn clippings for agricultural use
- Managed a team of four individuals to achieve course requirements and meet customer expectations

HONORS AND ACTIVITIES

- Student member, AIAA
- David G. Sant Engineering Scholarship Recipient – Utah State University
- 2018 Outstanding Undergraduate Researcher, Utah State Mechanical and Aerospace Engineering Department
- 2018 Outdoor Track and Field All-American
- Helen and John Lozar Graduate Assistantship Recipient
- Eagle Scout Award

CONFERENCE PRESENTATIONS

S. A. Whitmore, S. Fehlberg, R. Stoddard, “Direct Electroplating of Additive Manufactured Plastics for Hybrid Rocket Propulsion Systems,” 2018 Joint Propulsion Conference, AIAA Propulsion and Energy Forum, (AIAA 2018-4626).

S.A. Whitmore, B. Chamberlain, “Consumable Spacecraft Structures with Integrated, 3-D Printed Acrylonitrile Butadiene Styrene (ABS) Thrusters,” 53rd AIAA/SAE/ASEE Joint Propulsion Conference AIAA Propulsion and Energy Forum (AIAA 2017-4707).

S. Fehlberg, M. Örnek, T. Manship, S. Son, “The Effect of Encapsulated Nanoscale and Micron-scale Catalyst Particles on the Decomposition of Ammonium Perchlorate Crystals,” AIAA Propulsion and Energy Forum 2019 (AIAA 20194442)

JOURNAL PUBLICATION

S. Fehlberg, M. Örnek, T. Manship, S. Son, “Decomposition of Ammonium Perchlorate Encapsulated Nanoscale and Micron-scale Catalyst Particles,” In Preparation